

# VERIFIABLE MISSION PLANNING FOR SPACE OPERATIONS

Quentin Rommel<sup>\*†</sup>, Michael Hibbard<sup>\*‡</sup>, Pavan Shukla<sup>†</sup>, Himanshu Save<sup>§</sup>,  
Srinivas Bettadpur<sup>¶</sup>, and Ufuk Topcu<sup>¶</sup>

As space missions become more complex, planning methods must maximize mission performance while rigorously enforcing safety. We develop a probabilistic approach based on a finite-horizon Markov decision process to optimize spacecraft operations planning with safety guarantees. In the model, states capture essential mission parameters, and actions represent the operational adjustments needed to meet mission objectives. By directly incorporating uncertainties from environmental conditions and spacecraft dynamics, an optimal sequence of actions is computed that maximizes expected rewards and strictly enforces safety constraints. Numerical experiments on the GRACE-FO mission demonstrate robust performance under uncertainties while providing probabilistic safety guarantees, offering a reliable solution for autonomous spacecraft operations.

## INTRODUCTION

Spacecraft mission planning is increasingly challenged by the complex uncertainties inherent in space operations. Modern missions must perform high-precision observations while contending with unpredictable space weather, limited fuel reserves, and intricate orbital dynamics. Traditionally, mission planning relied on heuristic methods studying static scenarios to account for these uncertainties.<sup>1</sup> However, such approaches often fail to capture the full probabilistic nature of environmental variability and spacecraft dynamics, leading to suboptimal performance or potential safety violations.

Markov decision processes (MDP) provide a promising alternative. MDP is a mathematical framework for modeling planning and acting in stochastic environments with nondeterministic action selection.<sup>2</sup> An MDP models the system as a collection of states, actions, and probabilistic transitions, with each action yielding a corresponding reward. In the context of spacecraft mission planning, the system's states encapsulate key operational parameters—such as orbital altitude and fuel reserves—while the actions represent possible maneuvers or operational adjustments. By explicitly incorporating uncertainties, such as fluctuations in space weather and variations in orbital

\*Equal Contribution.

<sup>†</sup>Graduate Research Assistant, Department of Aerospace Engineering and Engineering Mechanics, The University of Texas at Austin, 2617 Wichita St, Austin, TX 78712.

<sup>‡</sup>Flight Algorithms Engineer, Starfish Space, 665 Andover Park W, Tukwila, WA 98188. (Work conducted as a Graduate Research Assistant, Department of Aerospace Engineering and Engineering Mechanics, The University of Texas at Austin, 2617 Wichita St, Austin, TX 78712.)

<sup>§</sup>Sr. Research Scientist, Center for Space Research, The University of Texas at Austin, 3925 W. Braker Lane, Suite 200, Austin, TX 78759.

<sup>¶</sup>Professor, Department of Aerospace Engineering and Engineering Mechanics, The University of Texas at Austin, 2617 Wichita St, Austin, TX 78712.

dynamics, MDPs enable the derivation of optimal policies that balance performance objectives with verifiable safety constraints.

The GRACE-FO mission<sup>3</sup> serves as a motivating scenario. Originally designed to measure Earth’s gravity field with high precision by flying two satellites in tandem, the mission soon faced critical setbacks when one accelerometer failed and a thruster leak emerged. Despite these challenges, GRACE-FO must maintain its primary objective by reducing atmospheric drag to preserve data quality and avoid resonant orbits—even though it operates on limited fuel and lacks provisions for altitude-raising maneuvers. Save et al.<sup>1</sup> introduced a traditional orbit management strategy for GRACE-FO that considers various solar activity scenarios; however, their method does not fully capture solar flux variability, sometimes resulting in premature reentry under worst-case conditions.

We propose to address these challenges by applying a finite-horizon MDP to space mission planning, which explicitly incorporates uncertainty into its state transitions. This framework enables adaptive policy synthesis that optimally schedules maneuvers based on probabilistic models of environmental conditions and spacecraft dynamics. In contrast to traditional scenario-based methods, the MDP-based approach continuously refines its decision-making process in response to real-time variations, thereby enhancing performance while rigorously enforcing safety constraints.

Prior studies on mission planning under uncertainty have explored various methods. Early scenario-based analyses, as presented by Save et al.,<sup>1</sup> relied on fixed worst-case, nominal, and best-case evaluations. However, this approach often results in overly conservative planning strategies. Recent work by Eddy et al.<sup>4</sup> applied MDPs to integrate uncertainty into the planning process, enabling dynamic balancing of multiple operational objectives. Other studies have taken alternative routes. Isaji and Ho<sup>5</sup> developed an integrated approach that combines stochastic programming with decomposition-based optimization to address both mission planning and spacecraft design under uncertainty. Vasile<sup>6</sup> leveraged evidence theory along with multi-agent collaborative search to generate robust mission designs by quantifying uncertain design parameters. Additionally, as explored by Ahmadi et al.,<sup>7</sup> risk-averse planning techniques incorporate dynamic coherent risk measures to synthesize policies that explicitly mitigate adverse outcomes.

We present a general framework for probabilistic mission planning and safety verification for spacecraft operations. First, a finite-horizon MDP framework is developed that directly embeds uncertainties into state transitions, enabling adaptive and real-time decision making. Second, we present how to verify the safety of the obtained strategy regarding some operational constraints. We then describe how to construct this MDP-based solution for the case of GRACE-FO. Finally, we show that it not only improves fuel efficiency and data quality but also provides measurable safety guarantees. These contributions extend traditional scenario-based methods<sup>1</sup> and build on dynamic MDP approaches,<sup>4</sup> offering a comprehensive and computationally efficient solution for robust spacecraft mission planning under uncertainty with safety guarantees.

## **PROBABILISTIC POLICY SYNTHESIS AND SAFETY VERIFICATION USING MARKOV DECISION PROCESSES**

A *Markov decision process* (MDP) is a common paradigm for modeling planning and acting in stochastic environments with nondeterministic action selection.<sup>2</sup> For mission planning, we focus on *finite-horizon* MDPs, wherein the decision-making process is performed over a finite number of time steps called a *planning horizon*. In the context of a spacecraft mission, the environment stochasticity could be due to, e.g., uncertainties in future space weather conditions, while actions

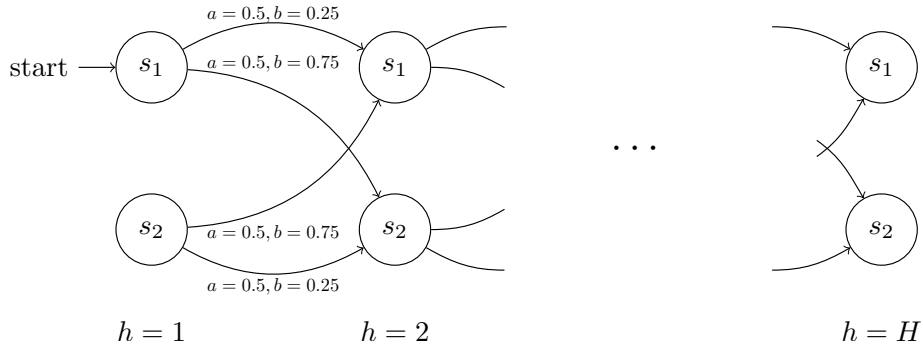


**Figure 1. A visualization of a simple finite-horizon MDP with horizon length  $H$ . The set of states is  $\mathcal{S} = \{s_1, s_2\}$**

and the set of actions is  $\mathcal{A} = \{a, b\}$ .

could correspond to performing altitude raises. Similarly, the planning horizon could be the operational lifetime of the mission, while individual time steps are specific points in time at which actions are chosen, e.g., daily, weekly, or monthly.

Formally, a finite-horizon MDP  $\mathfrak{M}$  is described by the tuple  $\mathfrak{M} = \langle \mathcal{S}, \mathcal{A}, \mathcal{H}, T, R, \mathbf{P}_0 \rangle$ , where  $s \in \mathcal{S}$  is a finite set of states,  $a \in \mathcal{A}$  is a finite set of actions,  $\mathcal{H} = \{0, 1, 2, \dots, h, \dots, H\}$  is a set of time indices with planning horizon  $H < \infty$ ,  $T : \mathcal{S} \times \mathcal{A} \times \mathcal{H} \times \mathcal{S} \rightarrow [0, 1]$ , is a transition function mapping state-action pairs at time step  $h$  to a probability distribution over successor states,  $R : \mathcal{S} \times \mathcal{A} \times \mathcal{H} \rightarrow \mathbb{R}$  is a reward function mapping state-action pairs at time step  $h$  to an associated reward, and  $\mathbf{P}_0 : \mathcal{S} \rightarrow [0, 1]$  is an initial state distribution. Let  $R(s, a, h)$  denote the reward obtained for selecting action  $a$  while in state  $s$  at time step  $h$ . Similarly, let  $T(s'|a, s, h)$  denote the probability of transitioning to state  $s'$  after taking action  $a$  while in state  $s$  at time step  $h$ . Note that since the transition function must define a valid probability distribution, we have  $\sum_{s' \in \mathcal{S}} T(s'|a, s, h) = 1$  for all  $(s, a, h) \in \mathcal{S} \times \mathcal{A} \times \mathcal{H}$ .

A visualization of a simple finite-horizon MDP is shown in Figure 1, where the planning horizon is of length  $H$ . The set of states is  $\mathcal{S} = \{s_1, s_2\}$ , the set of actions is  $\mathcal{A} = \{a, b\}$ , and the initial state is  $s_1$ . For the initial time step, each state-action pair is labeled by its associated transition probability, e.g.,  $T(s_2|s_1, b, 1) = 0.75$ . Intuitively, the transitions in the MDP flow only forward in time.

To resolve the nondeterminism in choosing an action, the decision-maker must synthesize a *time-dependent policy*  $\pi \in \Pi$  where  $\Pi$  is the set of time-dependent policies. Formally,  $\pi$  is a sequence of decision rules  $\{d_1, d_2, \dots, d_H\}$ , where each  $d_h : \mathcal{S} \times \mathcal{A} \rightarrow [0, 1]$  prescribes a probability distribution for action selection in each state at time step  $h$ . Notice that each decision rule is a function of only the current state of the decision-maker, rather than of its entire history of states. Such a policy is referred to as *Markovian*. Let  $\pi(a|s, h)$  denote the probability that action  $a$  is selected while in state  $s$  at time step  $h$  under policy  $\pi$ . If there exists an action  $a \in \mathcal{A}$  for each  $(s, h) \in \mathcal{S} \times \mathcal{H}$  such that  $\pi(a|s, h) = 1$  and  $\pi(a'|s, h) = 0$  for all  $a' \in \mathcal{A} \setminus a$ , we refer to  $\pi$  as *deterministic*. Finally, for a time-dependent policy, let  $\pi(s, h)$  denote the action selected deterministically while in state  $s$  at time step  $h$ .

Given the spacecraft mission environment expressed in terms of an MDP, we seek to determine whether there exists a policy that satisfies a given mission specification with probability at least  $1 - \delta$ . We want the spacecraft to always remain safe. In other words, it should never enter an unsafe

set, denoted as  $\mathcal{B} \subseteq \mathcal{S}$ . We require that the policy guarantees safety with a probability of at least  $1 - \delta$ . Here,  $\delta \in [0, 1)$  represents the maximum allowed chance of a safety violation. The safety probability requirement for a policy  $\pi \in \Pi$  associated to the specification  $\varphi$  can be written as:

$$\Pr^\pi(s_0 \models \Box \neg \mathcal{B}) \geq 1 - \delta, \quad (1)$$

where  $\Box \neg \mathcal{B}$  means ‘‘Always avoid  $\mathcal{B}$ ’’, and  $s_0 \in \mathcal{S}$  is the initial state of the MDP. Equivalently, since ‘‘always avoid  $\mathcal{B}$ ’’ is the opposite of ‘‘eventually reaching  $\mathcal{B}$ ’’, we can also write an equivalent reachability specification as:

$$\Pr^\pi(s_0 \models \Diamond \mathcal{B}) \leq \delta. \quad (2)$$

We assume that the mission of the spacecraft is to maximize the total expected reward collected over the planning horizon subject to a constraint that a mission safety specification  $\varphi$  must be satisfied with probability at least  $1 - \delta$ . We now formally state the problem of the decision-maker.

**Problem 1.** *Given an MDP  $\mathfrak{M}$  representing the spacecraft environment and a mission safety specification  $\varphi$ , synthesize a policy  $\pi^*$  that solves the following optimization problem.*

$$\max_{\pi \in \Pi} \quad \mathbb{E} \left[ \sum_{h=1}^H R(s, a, h) \right] \quad (3a)$$

$$\text{s.t.} \quad \Pr^\pi(s_0 \models \varphi) \geq 1 - \delta, \quad (3b)$$

where  $\Pr^\pi(s_0 \models \varphi)$  is the probability that the mission safety specification  $\varphi$  is satisfied under policy  $\pi$  starting in state  $s_0$  in MDP  $\mathfrak{M}$ .

This problem is solved in two steps. First, the policy  $\pi \in \Pi$  for the objective (3a) is synthesized without considering the constraint (3b). Formally,

$$\pi^* = \arg \max_{\pi \in \Pi} \mathbb{E} \left[ \sum_{h=1}^H R(s, a, h) \right]. \quad (4)$$

$\pi^*$  is obtained by solving the recursive Bellman equations backwards-in-time according to

$$V^*(s, H) = \max_{a \in \mathcal{A}} [R(s, a, H)] \quad \forall s \in \mathcal{S}, \quad (5a)$$

$$V^*(s, h) = \max_{a \in \mathcal{A}} \left[ R(s, a, h) + \sum_{s' \in \mathcal{S}} T(s'|s, a, h) V^*(s', h+1) \right] \quad \forall (s, h) \in \mathcal{S} \times \mathcal{H} \setminus H, \quad (5b)$$

where  $V^*(s, h)$  is the optimal *value function* for state  $s$  at time step  $h$  and  $\pi^*(s, h)$  is the corresponding maximizing value of  $a \in \mathcal{A}$ . We then evaluate the safety performance of the obtained policy  $\pi$ . To do this, we define  $V^\varphi(s, h) = \Pr^\pi((s, h) \models \Box \neg \mathcal{B})$ . Note that here  $\pi$  is the policy obtained from solving the unconstrained problem (4). The safety value function  $V^\varphi(s, h)$  is computed using the following formulation:

$$V^\varphi(s, h) = \begin{cases} 0, & \text{if } s \in \mathcal{B}, \\ 1, & \text{if } s \notin \exists \Diamond \mathcal{B}, \\ \max_{a \in \mathcal{A}} \sum_{s' \in \mathcal{S}} T(s'|s, a, h) V^\varphi(s', h+1), & \text{otherwise,} \end{cases} \quad (6)$$

with an appropriate terminal condition at  $h = H$  (i.e. for  $s \notin \mathcal{B}$ ,  $V^\varphi(s, H) = 1$  if no further transitions occur). A policy is considered feasible if it guarantees that the safety probability at the initial state is at least  $1 - \delta$ :

$$V^\varphi(s_0, 0) \geq 1 - \delta, \quad (7)$$

ensuring that the spacecraft remains safe with the required probability starting from  $s_0$ .

To model the safety specification  $\varphi$ , we can characterize it in terms of a *temporal logic formula*.<sup>8,9</sup> The foundational building blocks of a temporal logic formula are *atomic propositions*, which evaluate to either `true` or `false`, e.g., “*the spacecraft has nonzero fuel reserves remaining.*”

Note that it is straightforward to generalize the constraint (13b) to the probability of multiple mission specifications. We refer the reader to,<sup>10</sup> section 8 for further details.

## ENVIRONEMENT DEFINITION

Transitioning from the MDP formulation to a detailed representation of the operational environment is crucial for accurate policy synthesis. Although the MDP framework guides decision making under uncertainty, its effectiveness relies on a clear understanding of the forces affecting spacecraft motion. Orbital mechanics forms the foundation for modeling a spacecraft’s trajectory by accounting for gravitational forces, atmospheric drag, and other perturbations, which in turn define the deterministic states, actions, and transitions in our MDP. At the same time, space weather conditions directly impact the environment in which the spacecraft operates, yet their inherent variability makes them very difficult to predict accurately. These uncertainties are incorporated into the transition probabilities of the model.

### Orbital Mechanics

Consider a spacecraft in an elliptical orbit around the Earth. Let  $\mathbf{r}(t) = [\mathbf{p}(t)^\top, \mathbf{v}(t)^\top]^\top \in \mathbb{R}^6$  denote the Cartesian state of a spacecraft in the inertial frame, where  $\mathbf{p}(t) = [x(t), y(t), z(t)]^\top$  and  $\mathbf{v}(t) = [\dot{x}(t), \dot{y}(t), \dot{z}(t)]^\top$  are the spacecraft position and velocity at time instant  $t$ . In what follows, we will omit the time index  $t$  for notational clarity. Assuming a spherical Earth, the altitude  $R_{\text{alt}}$  of the spacecraft above Earth’s surface can subsequently be obtained from its position  $\mathbf{p}$  according to

$$R_{\text{alt}} = \|\mathbf{p}\|_2 - R_e, \quad (8)$$

where  $R_e$  is the radius of the Earth.

The dynamics of the spacecraft are given by

$$\ddot{\mathbf{r}} = -\mu \frac{\mathbf{r}}{\|\mathbf{r}\|_2^3} + F_{\text{drag}} + F_{\text{pert}}, \quad (9)$$

where  $\mu$  is the gravitational parameter of the Earth,  $F_{\text{drag}}$  is the atmospheric drag force, and  $F_{\text{pert}}$  is the combination of the remaining perturbing forces acting on the spacecraft. The term  $F_{\text{pert}}$  could include, for example,  $J_2$  and  $J_3$  effects. The atmospheric drag term  $F_{\text{drag}}$  is equal to

$$F_{\text{drag}} \triangleq -\frac{1}{2} C_d \frac{A}{m} \rho A v_a v_a, \quad (10)$$

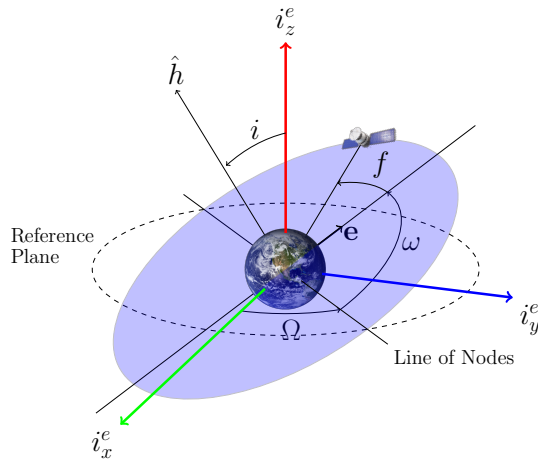


**Figure 2. Visualization of the Keplerian orbital elements.**

where  $C_D$  is the drag coefficient of the spacecraft,  $A$  is the cross-sectional area of the spacecraft,  $m$  is the mass of the spacecraft,  $\rho_A$  is the altitude-dependent atmospheric density, in  $\text{kg}/\text{km}^3$ ,  $v_a$  is the velocity of the spacecraft relative to the Earth-fixed frame, given by

$$v_a \triangleq \begin{bmatrix} \dot{x} + \dot{\theta}y \\ \dot{y} - \dot{\theta}x \\ \dot{z} \end{bmatrix}, \quad v_a = \|v_a\|_2,$$

in which  $\dot{\theta}$  is the rotation rate of the Earth. Here, we use the MSIS atmosphere model<sup>111213</sup> to compute the value of  $\rho_A$  as a function of the altitude, and the solar flux at 10.7 cm (F10.7) using NOAA prediction.<sup>14</sup>

In tandem with the preceding Cartesian representation of the spacecraft dynamics, one can instead characterize its orbit in terms of the Keplerian orbital elements  $\{a, e, i, \omega, \Omega, f\}$ , where  $a$  is the semimajor axis length of the elliptical orbit,  $e \in [0, 1)$  is the eccentricity of the orbit,  $i$  is the inclination of the orbit,  $\omega$  is the argument of periape,  $\Omega$  is the longitude of the ascending node, and  $f$  is the true anomaly.<sup>15</sup> These orbital elements are visualized in Figure 2, where the angles are defined with respect to the Earth-centered inertial (ECI) reference frame. We refer the reader to<sup>15</sup> for information on how to convert between the Cartesian and Keplerian representations of the spacecraft state.

## Space Weather Conditions

Due to the atmospheric drag force  $F_{\text{drag}}$ , the eccentricity and semimajor axis of the spacecraft orbit decrease monotonically over its operational lifetime, eventually approaching values of  $R_e$  (Earth's radius) and zero, respectively. As a result, the spacecraft gradually descends to a circular orbit of zero altitude.<sup>15</sup> The extent and variability of this degradation depend heavily on the atmospheric density at the spacecraft's altitude, which is strongly influenced by solar activity.

The solar cycle governs the Sun's activity levels and, in turn, the atmospheric environment encountered by the spacecraft. However, the duration and intensity of individual cycles vary; larger cycles tend to last longer than 11 years, while smaller cycles are typically shorter. Solar activity

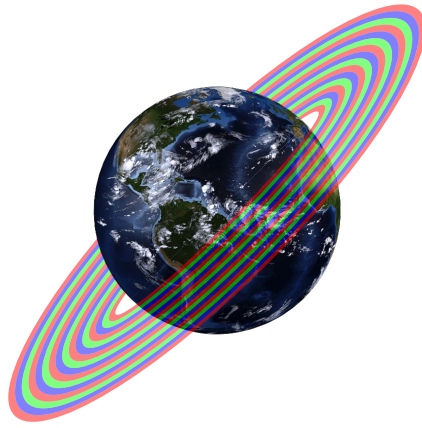


**Figure 3.** We construct the discrete representation of the mission environment by sampling a representative set of mean orbits.

is commonly categorized into three levels: high, moderate, and low.<sup>1</sup> During high solar activity, increased ultraviolet and X-ray radiation heats and expands the Earth's upper atmosphere, raising atmospheric density at orbital altitudes and increasing drag forces. This accelerates orbital decay, requiring more frequent station-keeping maneuvers and increasing fuel consumption. In moderate activity periods, atmospheric density variations are less extreme, allowing for more stable orbit maintenance. Conversely, low solar activity leads to reduced drag, minimizing fuel expenditure and extending mission lifetime.

The variability in solar activity across different cycles can be incorporated into the MDP transition model by defining states and transitions that reflect the probabilistic nature of future solar activity levels. Since larger solar cycles exhibit prolonged high-drag conditions, while smaller cycles may allow for extended low-drag periods, transitions between states can be weighted using historical solar cycle data. By integrating probabilistic dependencies into the MDP, the model allows for dynamic adjustments in altitude control, optimizing fuel usage, and ensuring prolonged mission operation under different space weather conditions.

## **CASE STUDY**

Using the MDP theory and the described dynamics, we now present how to construct the MDP model that will be used in solving Problem 1 in the context of the GRACE-FO mission.

### **GRACE-FO mission**

The NASA Gravity Recovery and Climate Experiment (GRACE) mission, launched in 2002, was a NASA mission that sought to obtain high-accuracy estimates of Earth's gravity field via high-resolution spatial and temporal measurements.<sup>16</sup> The mission consisted of a pair of spacecraft, named GRACE-1 and GRACE-2, operating in near-circular orbits at an inclination of 89.5 degrees and an altitude of approximately 500 kilometers.

The GRACE-FO (Gravity Recovery and Climate Experiment Follow-On) mission, launched in May 2018, continues the legacy of the original GRACE mission to measure Earth's gravity field with unprecedented precision. By monitoring variations in the inter-satellite range using K-Band Ranging and Laser Ranging Interferometer technologies, GRACE-FO provides critical data on global

surface mass changes.

One major challenge arises from the failure of the accelerometer on GRACE-FO 2 (GF2), rendering it unable to directly measure non-gravitational forces. To compensate, data from the accelerometer of GRACE-FO 1 (GF1) is transplanted to GF2, relying on the assumption that the environmental conditions experienced by both satellites are nearly identical within a 24-30-second delay. Although this method captures over 99% of the non-gravitational forces, it introduces signal-proportional errors amplified in high-drag environments, degrading the accuracy of derived gravity fields. Furthermore, the exact nature of the current solar cycle is uncertain; it could exhibit high, moderate, or low activity, each scenario presenting different levels of atmospheric drag. To address these uncertainties, we aim to develop a robust strategy that accounts for the different scenarios of solar activity and their influence on atmospheric drag, ensuring reliable mission operations and data quality.

Another critical issue involves a small leak in the cold-gas thrusters used for orbit maintenance. Every use of the thrusters risks worsening the leak, potentially increasing the rate of fuel loss and compounding the challenge of preserving enough fuel for critical operations. This creates a dynamic trade-off between performing necessary station-keeping maneuvers and avoiding actions that might accelerate the leak, further threatening the mission's longevity and scientific output.

The objective is to develop a strategy to optimize GRACE-FO's mission time and scientific output under these constraints. We explicitly account for uncertainties in space weather and fuel availability, including the impact of solar cycle variability and the thruster leak.

## State Modeling

We discretize the environment of the spacecraft in a pair of dimensions. The first of these dimensions is the altitude of the spacecraft. Recall that we are primarily interested in the effect of solar flux on atmospheric drag, and that atmospheric drag only affects the semimajor axis length and the eccentricity of the spacecraft orbit. Furthermore, since the GRACE mission is nominally in a circular orbit (i.e.  $e = 0$ ), its eccentricity is unaffected by atmospheric drag and remains constant over time. Thus, we focus solely on discretizing the altitude of the spacecraft (which is a function of the semimajor axis length as given by (8)).

To construct this discretization, let  $a_{min}, a_{max} \in \mathbb{R} \geq 0$ ,  $a_{max} > a_{min}$ , be a minimum and maximum altitude, respectively, and  $N_a \in \mathbb{Z}$  denote the number of discrete altitudes to consider within these bounds. Denote the set of these discrete altitudes by  $\mathcal{S}_a \triangleq \{a_{min} + \frac{R_a}{2}, a_{min} + \frac{3R_a}{2}, \dots, a_{max} - \frac{R_a}{2}\}$ , where  $R_a \triangleq \frac{a_{max} - a_{min}}{N_a}$ . Each altitude  $s \in \mathcal{S}_a$  corresponds to a discrete band centered around  $s$ , i.e., the band  $[s - \frac{R_a}{2}, s + \frac{R_a}{2}]$ , as shown in Figure 3. Although the true semimajor axis length of the spacecraft will not generally reside on one of the sampled altitudes  $s \in \mathcal{S}_a$ , we can instead bin it into a corresponding band (assuming that it lies within the minimum and maximum altitudes).

The second discretization is in the temporal dimension. Particularly, given a mission planning horizon  $H \in \mathbb{R}$  (nominally expressed in units of seconds) and a number of discrete time steps  $N_H \in \mathbb{Z}$ , let  $\mathcal{H} \triangleq \{0, \frac{H}{N_H}, \frac{2H}{N_H}, \dots, \frac{(N_H-1)H}{N_H}\}$  denote the set of discrete time indices. In what follows, it is assumed that decisions can only be made at time instants belonging to the set  $\mathcal{H}$ .

To construct the fuel discretization, we use a similar method as for the altitude. Let  $f_{min}, f_{max} \in \mathbb{R}_{\geq 0}$ , with  $f_{max} > f_{min}$ , be the minimum and maximum fuel levels, respectively, and let  $N_f \in \mathbb{Z}$



denote the number of discrete fuel levels to consider within these bounds. We denote the set of these discrete fuel levels by  $\mathcal{F} \triangleq \{f_{min} + \frac{R_f}{2}, f_{min} + \frac{3R_f}{2}, \dots, f_{max} - \frac{R_f}{2}\}$ , where  $R_f \triangleq \frac{f_{max} - f_{min}}{N_f}$ . Following the same procedure as stated for the altitude, the true fuel level of the spacecraft is binned into the corresponding fuel band.

## Reward Modeling

At a high level, the objective of the GRACE mission is to provide high-quality observations of changes in Earth's gravitational field.<sup>17</sup> The quality of these observations generally increases with lower atmospheric density, which occurs at higher altitudes. Due to this fact, the reward function  $R$  should be independent of the choice of the action selection and only a function of the current state (i.e., altitude) and time step of the mission. The dependence of the reward function  $R$  on time could be due to, e.g., time-varying atmospheric conditions that affect the observation quality. Thus, we introduce  $R(s, :, h) \triangleq R(s, a, h)$  for all  $a \in \mathcal{A}$  to denote the reward (a function of the observation quality) for being in a state  $s \in \mathcal{S}$  corresponding to a fixed, discrete altitude. In other words,  $R(s, :, h)$  is independent of the action taken. Note that  $R(s, :, h)$  should be non-negative and monotonically increasing as the corresponding altitude of  $s$  increases.

An additional hindrance to observation quality is the existence of *resonant orbits*, which are orbits with a periodic ground track.<sup>18</sup> Due to the periodicity of this ground track, less of Earth's surface is observed, reducing the quality of the global gravitational field estimation. Thus, for any discrete altitude state  $s \in \mathcal{S}_a$  for which a resonant orbit exists in its corresponding altitude band  $[s - \frac{R_a}{2}, s + \frac{R_a}{2}]$ , we can set  $R(s, :, h) = 0$ . Alternatively, given periodicity of the resonant orbit  $i$ ,  $res_i$  (i.e., the rate at which the ground track repeats), one can scale the reward function by a multiplicative factor  $\alpha < 1$  to account for variations in the reduction of observation quality. The reward function can then be defined as

$$R(s, :, h) = \mathbb{E} \left[ alt_{h+1} \left( \prod_{i=1}^N \left( \alpha \frac{res_i}{res_{max}} + \beta \right) \right)^{\frac{1}{N}} \right], \quad (11)$$

Here,  $alt_{h+1}$  denotes the spacecraft's altitude at the next time step,  $N$  is the number of resonant orbits encountered until that step, and  $res_i$  represents the repetition rate of the  $i$ th resonant orbit, normalized by  $res_{max}$ , the maximum possible repetition rate.  $\alpha$  scales the normalized repetition rate to penalize high resonance, while  $\beta$  provides an offset to ensure that the penalty does not reduce the reward excessively. Taking the geometric mean (by raising the product to the power of  $\frac{1}{N}$ ) aggregates the multiplicative penalties, and the expectation  $\mathbb{E}[\cdot]$  accounts for uncertainty in the next altitude and resonance effects, thus balancing the benefits of increased altitude with the degradation in observation quality due to repetitive ground tracks. A visualization of the process for setting the reward for being in a discrete altitude state  $s \in \mathcal{S}_a$  is shown in Figure 4.

Resonant orbits are computed by enforcing the repeat ground track condition

$$D \cdot T_{sat} = N \cdot T_{nodal},$$

where  $D$  and  $N$  denote the number of satellite revolutions and nodal days, respectively. Here, the satellite's nodal period is given by

$$T_{sat} = \frac{2\pi}{n + \dot{\omega}},$$

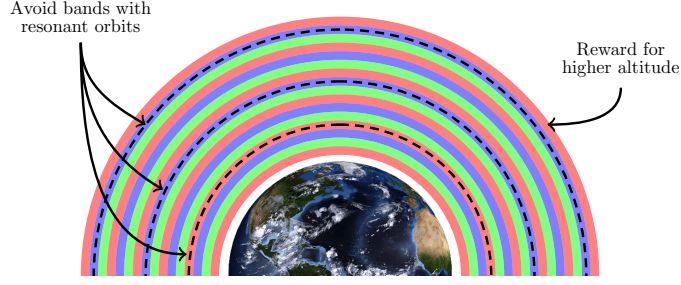


**Figure 4. Visualization for the shaping of the reward function  $R$ .**

where  $n$  is the mean motion and  $\dot{\omega}$  is the perigee precession rate. The Earth's nodal period is expressed as

$$T_{\text{nodal}} = \frac{2\pi}{\omega_e - \dot{\Omega}}.$$

where  $\omega_e$  is the Earth's rotation rate and  $\dot{\Omega}$  is the nodal precession rate.

Substituting these into the resonance condition yields

$$\frac{D}{n + \dot{\omega}} = \frac{N}{\omega_e - \dot{\Omega}}.$$

Since the mean motion  $n$  is directly related to the semi-major axis via Kepler's law, this equation is solved iteratively using the Lagrange Planetary Equations with Klokočník's method.<sup>19</sup> We then obtain the resonant altitudes. The resulting normalized repetition rate is then incorporated into the reward function (11).

### Action and Fuel Cost Modeling

There are several choices to model the discrete set of actions  $\mathcal{A}$  for the GRACE mission. At their core, these actions represent the choice of how much altitude to gain over the subsequent discrete time interval. For example, if the temporal discretization is fine enough, then a single, continuous burn could be approximated by a sequence of smaller burns performed at each discrete time step. In this case, the set of actions is  $\mathcal{A} = \{no\ burn, +R_a\}$ , where  $+R_a$  denotes the choice to increase the altitude by  $R_a$ . Since the bands are assumed to be evenly spaced in altitude, this action corresponds to transitioning to the state  $s' \in \mathcal{S}$  such that the altitude of  $s'$  is equal to the altitude of  $s$  plus  $R_a$ . For models with lower temporal resolution, multiple actions corresponding to a finite set of altitude increases can be included in the set  $\mathcal{A}$ , i.e.,  $\mathcal{A} = \{no\ burn, +R_a, +2R_a, \dots, +N_A R_a\}$ , where  $N_A R_a$ ,  $N_A \in \mathbb{Z}$ , is the maximum one-step orbit increase. A visualization of such a set  $\mathcal{A}$  is shown in Figure 5, where there exist a set of seven possible actions (no burn and six possible altitude increases). The selected action is in black. A third option for the choice of action is to use a geometric set to approximate the choice of increasingly large fuel burns. Specifically, let  $\hat{\gamma} > 1$  be a constant scaling factor and  $N_A$  be the number of actions. Then,  $\mathcal{A}$  corresponds to the altitude increase  $\{no\ burn, +[\hat{\gamma}^0]R_a, +[\hat{\gamma}^1]R_a, \dots, +[\hat{\gamma}^{N_A-1}]R_a\}$ .

Associated with each action is a fuel cost, while the decision-maker must ensure that the cumulative fuel cost throughout the mission does not exceed its fuel budget. Let us denote the fuel cost when taking action  $a \in \mathcal{A}$  while in a state  $s \in \mathcal{S}$  by  $C(s, a)$  and the fuel budget by  $C_{\text{max}}$ . Trivially,

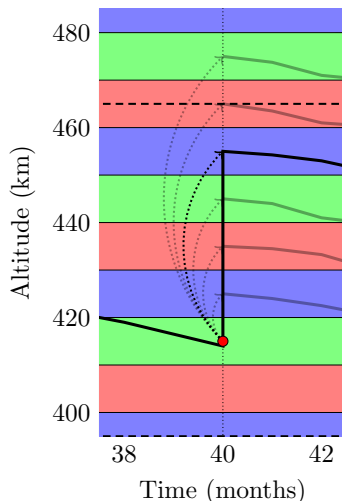


**Figure 5. Visualization of the set of feasible actions  $\mathcal{A}$ , which correspond to different instantaneous altitude gains.**

for the action corresponding to *no burn*, the fuel cost is zero. For the remaining actions, there exist several options for modeling the fuel costs and the fuel budget. These options are as follows.

1. *Maximum Altitude Change.* As previously discussed, each action is associated with an increase in the operational altitude of the GRACE mission. The cost of an action is its corresponding altitude increase, i.e.,  $C(s, +nR_a) = +nR_a$  for all  $n \in \{1, \dots, N_A\}$ . Similarly, the fuel budget is a maximum cumulative altitude increase over the mission horizon.
2. *Fuel usage,  $\Delta v$ .* Associated with each action in each state is a corresponding fuel usage, encoded by the  $\Delta v$  required to complete the altitude change. The fuel budget is a maximum cumulative  $\Delta v$  usage over the mission horizon. Due to changes in atmospheric density over time (such as due to varying solar flux), the fuel cost is likewise time-varying, which we express by  $C(s, +nR_a, h)$ .

## Transition Modeling

Several layers of stochasticity exist in the mission environment. The first of these layers is the future uncertainty in the solar flux level, i.e., whether the next solar cycle will result in low, medium, or high solar flux. Denote each of these probabilities by  $\Pr_{low}$ ,  $\Pr_{med}$ , and  $\Pr_{high}$ , respectively.

The second layer of uncertainty is that the solar flux over time for a fixed solar cycle intensity level is also stochastic. Denote the probability of a given value of the solar flux  $f$  being realized given a fixed solar cycle intensity by  $\Pr(f|i)$ , where  $i \in \{low, medium, high\}$ . As previously discussed, the solar flux affects atmospheric density, which in turn affects the drag coefficient  $C_D$ . The larger the coefficient of drag, the more quickly the altitude decays. Thus, the rate of altitude decay is a random variable that is dependent on the current solar flux. Assuming an instantaneous altitude

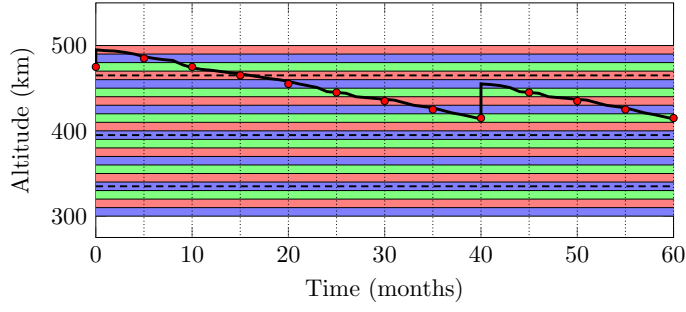


**Figure 6.** Example visualization of the evolution of the mission altitude over the planning horizon.

change, for a given state-action pair, we can then populate the transition probabilities according to

$$T(s'|s, a, h) = \quad (12a)$$

$$\Pr(\text{alt}_{h+1} \in [R_{s'} - \frac{R_a}{2}, R_{s'} + \frac{R_a}{2}] | \text{alt}_h = R_s + {}^+R_a) = \quad (12b)$$

$$\sum_{i \in \{low, medium, high\}} \Pr_i \int_f \Pr(f|i) \cdot \Pr(\text{alt}_{h+1} \in [R_{s'} - \frac{R_a}{2}, R_{s'} + \frac{R_a}{2}] | \text{alt}_h = R_s + {}^+R_a, f) df, \quad (12c)$$

where  $R_s$  is the altitude corresponding to state  $s \in \mathcal{S}$  and  ${}^+R_a$  is the altitude gain corresponding to selecting action  $a \in \mathcal{A}$ . Note that (12c) is obtained from (12b) by explicitly including the conditioning of the transition probability on the solar flux. Furthermore, since the state dynamics themselves are assumed to have no stochastic disturbances,  $\Pr(\text{alt}_{t+1} \in [R_{s'} - \frac{R_a}{2}, R_{s'} + \frac{R_a}{2}] | \text{alt}_t = R_s + {}^+R_a, f)$  takes either a value of 0 or 1 (i.e., it is binary). In practice, the integral over  $f$  can be numerically approximated and the state transition matrix used to efficiently compute the subsequent altitude. A visualization of an example trajectory (with respect to the mission altitude) is shown in Figure 6.

Note that decision are only made at the discrete time instances represented by the densely dotted vertical lines. Furthermore, the mission altitude will not generally reside on one of the discretely sampled states  $s \in \mathcal{S}$ . However, given a set  $\mathcal{S}$  sufficiently densely sampled from the set of feasible altitudes  $[a_{min}, a_{max}]$ , binning the actual altitude into the corresponding band should provide a good approximation of the continuous dynamics.

In general, a single continuous burn using all remaining fuel is the optimal action to maximize the operational lifetime of the mission. However, such an action lacks any robustness as no fuel remains aboard the spacecraft to address any potential changes to the mission plan. Several possibilities to increase the strategy robustness are listed as follows:

- (i) **Collision avoidance.** When the risk of collision with another spacecraft or orbital debris increases, GRACE cannot execute effective avoidance maneuvers. This risk is quantified by a collision rate,  $\lambda_c$ , whose integration over discrete time intervals yields the probability that a collision avoidance maneuver is required.
- (ii) **Station keeping.** In order to maintain the desired orbit, the spacecraft must conserve fuel

against perturbing forces that affect not only altitude but also other orbital parameters such as inclination. This requirement is managed by imposing a maximum fuel budget constraint.

- (iii) **Fuel leaks.** A critical failure in the fuel system may render the remaining fuel unusable. The likelihood of such a fuel leak is expressed by a fuel failure rate,  $\lambda_f$ , whose integration over each time interval determines the probability of a leak occurring.
- (iv) **Uncertain thrust.** Variability in the thruster system leads to differences between the actual thrust,  $Th_a$ , and the commanded thrust,  $Th_c$ . This variability is modeled by a probability distribution  $p_{Th}(Th_a)$ , which captures the likelihood of various thrust values in response to  $Th_c$ . By integrating this distribution over the time intervals during which thrust is applied, one quantifies the overall impact of thrust uncertainty on maneuver performance. This probability is then incorporated into the state transition model to manage the effects of uncertain thrust.

For the GRACE-FO mission, only thrust uncertainty is considered. Fuel leaks predominantly result from the attitude control system, which operates daily, so orbit-raising maneuvers have little effect on them. In addition, the spacecraft employs its attitude control system for all maneuvers, and no extra fuel is reserved for station keeping or collision avoidance, as these events were not part of the original design.

### Problem Formulation

We now formalize the mission planning problem as an optimization task over a finite planning horizon. The objective is to maximize the total expected reward while ensuring that a critical safety specification is satisfied with high probability. We define a safety requirement expressed as a time logic formula that captures two key constraints:

1. The spacecraft must not perform maneuvers more frequently than every three months.
2. The spacecraft must never drop below an altitude of 300 km.

The optimization problem is formulated as follows:

$$\max_{\pi} \quad \mathbb{E} \left[ \sum_{h=1}^H R(s, a, h) \right] \quad (13a)$$

$$\text{s.t.} \quad \Pr^{\pi}(s_0 \models \varphi) \geq 1 - \delta, \quad (13b)$$

where  $R(s, a, h)$  is the reward obtained at time step  $h$ ,  $s_0$  is the initial state,  $\varphi$  is the TL safety specification, and  $\delta$  denotes the maximum allowable probability of a safety violation.

The informal safety specification can be read as follows:

*”The spacecraft does not perform a maneuver more often than every 3 months, and it never drops below 300 km.”*

To encode this requirement formally in a temporal logic specification, we define the following atomic propositions:

- `maneuver`: Evaluates to `true` when the spacecraft performs a maneuver at the current time step.
- `altitude300`: Evaluates to `true` when the spacecraft’s altitude is below 300 km.

A possible temporal logic formula is:

$$\Box \left[ (\text{maneuver} \rightarrow \neg(X \text{maneuver} \vee XX \text{maneuver})) \wedge \neg \text{altitude300} \right], \quad (14)$$

which reads as: “It is always the case that if a maneuver is executed, no maneuver is performed in the next two time steps, and the spacecraft’s altitude remains above 300 km.”

This formulation guarantees that maneuvers are sufficiently spaced in time and that the spacecraft operates within the safe altitude range throughout the mission.

## EXPERIMENTAL RESULTS

The proposed planning method is applied to the GRACE-FO mission, which we assume is scheduled to operate from May 2018 until December 2029. This operating period provides an extra year beyond the planned launch of GRACE-C in December 2028 to accommodate possible launch delays or initial measurement issues. At the start of the mission, the spacecraft is positioned at an altitude of 490 km and is allocated 5 kg of fuel for orbit-raising maneuvers.

The discretizations form the basis of the MDP model, in which each state is defined by the discretized altitude, fuel level, and time since the last maneuver. The available actions correspond to the feasible altitude changes. Accurate capture of small changes in altitude is achieved by dividing the altitude range between 300 km and 500 km into 1500 intervals. The fuel level is discretized into 500 states to model fuel consumption precisely. An additional state variable tracks the time elapsed since the last maneuver; this enforces the safety requirement for sufficient spacing between maneuvers. An action can be taken every month. To accommodate the low temporal resolution, the available maneuvers are chosen using a geometric progression, which permits various magnitudes of altitude increases.

### Deterministic Planning

In the first set of simulations, the solar flux is assumed to be fixed at its expected value (as provided by NOAA<sup>14</sup>), and the cost for performing an orbit-raising maneuver is treated as deterministic. With these assumptions, the MDP is solved using a backward-recursion scheme. Figure 7 illustrates the deterministic evolution of altitude and fuel consumption. In this simulation, the spacecraft’s altitude increases in steps, reaching a final altitude slightly below 450 km, while maneuvers occur approximately every 6 months. These results indicate that the solution consistently maintains the spacecraft above 300 km.

In contrast, traditional mission planning methods typically schedule maneuvers at fixed intervals without considering the current state of the spacecraft. Such classic approaches spread maneuvers evenly over time, which can lead to unnecessary fuel consumption or insufficient altitude control. The MDP-based method, however, adapts the timing and magnitude of maneuvers based on the current altitude and fuel level. This dynamic scheduling helps to optimize fuel usage while ensuring that safety requirements are met more consistently.

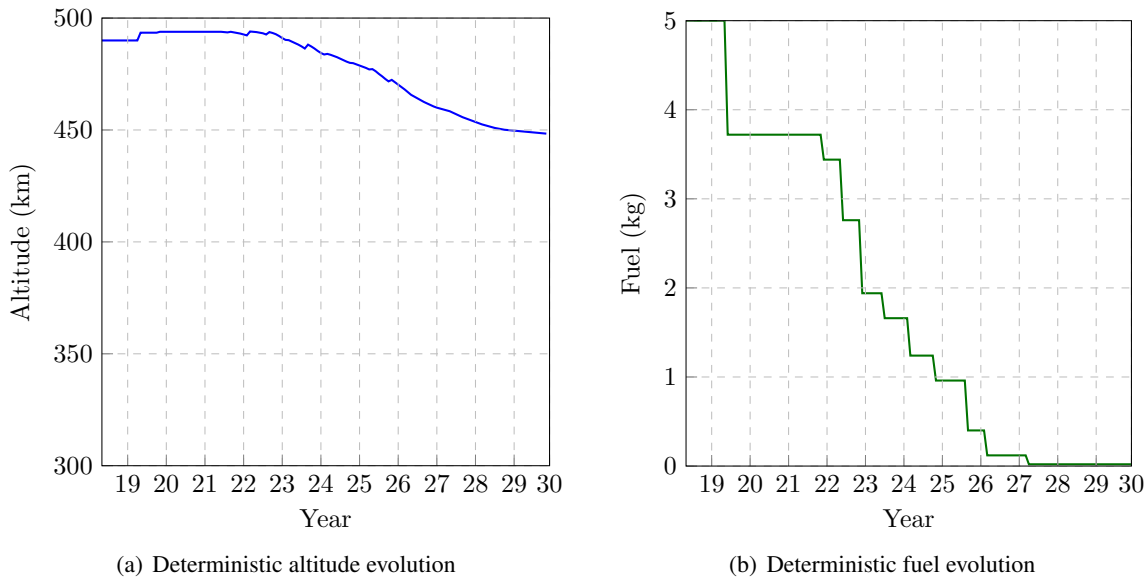


**Figure 7. Deterministic altitude and fuel evolution (bottom) when solving the MDP with deterministic transitions.**

### Planning Under Uncertainties

Next, we incorporate uncertainties into the model by treating both the solar flux and the outcomes of the orbit-raising maneuvers as random variables. Figure 8 shows the evolution of the solar flux over time, with the 75% quartile range highlighted in orange; these discretized distributions are integrated into the model. We then evaluate state transitions by considering best-case, worst-case, and average scenarios based on variations in solar flux and orbit-raising cost. Figure 9 displays a range of possible trajectories for altitude and fuel consumption. As expected, the worst-case scenario leads to fuel depletion early in 2025, while the best-case scenario extends fuel availability until 2029. The final altitude varies widely—from below 300 km up to 475 km—with an average of 410 km. Although the average behavior appears to satisfy the temporal specification, this plot alone does not provide full probabilistic safety guarantees. It suggests possible violations of the requirement that the altitude remains above 300 km. We therefore now turn to safety verification.

### Safety Verification

We study the satisfaction of the safety requirement by computing the value function associated with the temporal logic specification. It ensures that the altitude never falls below 300 km and that maneuvers are not executed too frequently. Figure 10 shows the probability distribution for the final altitude and its cumulative density function. The results demonstrate that the probability of falling below 300 km is nearly zero, with a 95% chance that the final altitude will exceed 425 km. Analysis of the optimal policy further confirms that if a maneuver occurs within a recent period (specifically, within the last 6 months), no additional orbit-raising maneuver is scheduled.

These results underscore the strength of the MDP framework in enforcing strict safety constraints while optimizing performance. Unlike traditional planning methods that do not explicitly verify safety through continuous feedback, the value function in this approach provides a clear measure of safety compliance. The near-zero risk of dropping below the minimum altitude and the high

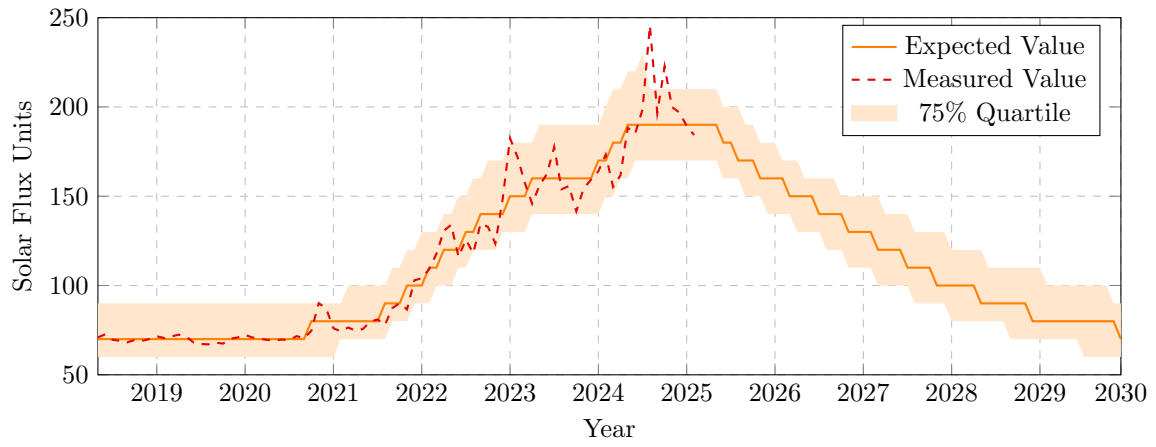
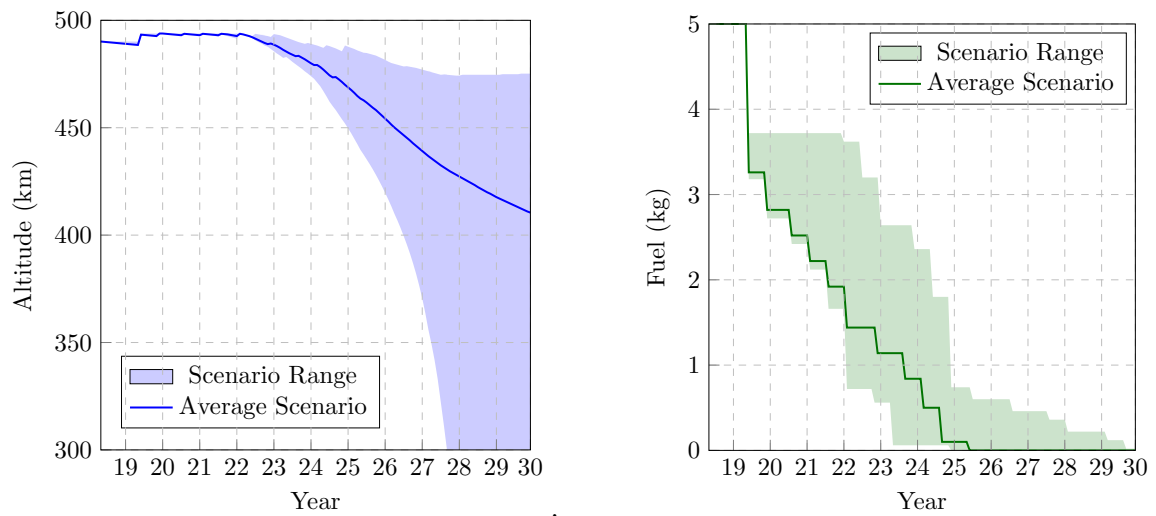


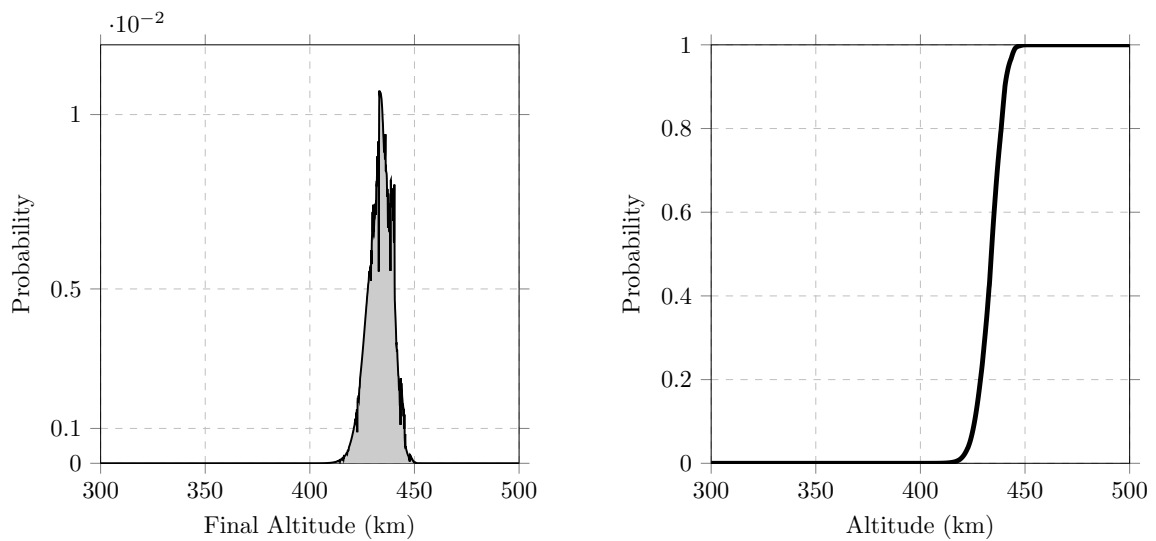
**Figure 8. Solar flux evolution**



(a) Altitude evolution with uncertainties

(b) Fuel evolution with uncertainties

**Figure 9. Altitude and fuel evolution when solving the MDP with uncertain transitions,**



(a) Probability distribution for the final altitude

(b) Cumulative distribution for the final altitude

**Figure 10. Probabilistic verification for the final altitude following the policy  $\pi$  using the initial condition of GRACE-FO at its launch.**



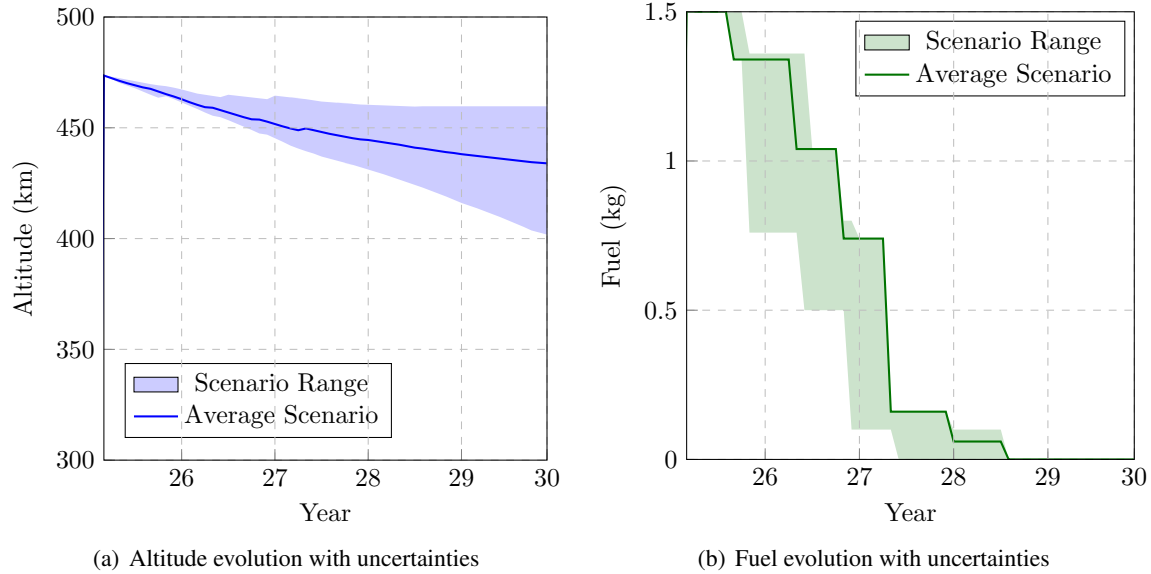


**Figure 11. Altitude and fuel evolution when solving the MDP with uncertain transitions using GRACE-FO state in March 2025 as the initial condition.**

probability of maintaining an altitude above 425 km indicate that the adaptive policy not only meets but exceeds safety requirements.

### Current-State Planning

The MDP formulation updates the optimal action as more accurate solar flux data becomes available. This capability enables the computation of an optimal policy for orbit-raising maneuvers that adapts to the current state of the GRACE-FO spacecraft. For example, in February 2025, when only 1.5 kg of fuel remains, the same policy computes an updated sequence of maneuvers. As shown in Figure 11, the resulting strategy clearly meets the safety specification: the policy keeps the spacecraft’s altitude well above 300 km and prevents an additional maneuver if one has been executed within the past three months, following the same principles as the full mission planning.

These current-state experiments highlight the method’s ability to adapt under critical fuel constraints. Unlike traditional approaches that schedule maneuvers at fixed intervals, the MDP-based policy adjusts its actions dynamically based on real-time state information. This adaptive behavior ensures that even when fuel is scarce, the spacecraft operates safely and efficiently. Overall, the experiments provide strong evidence that the planning method remains robust under uncertainties in the environment, effectively handling unpredictable variations in solar flux and maneuver costs while maintaining operational safety.

### CONCLUSION

We have developed a probabilistic framework that integrates mission planning with safety verification by modeling spacecraft operations as a finite-horizon Markov decision process. We have applied this method to the GRACE-FO mission scenario and have demonstrated that it produces robust and optimal sequences of actions under both deterministic and stochastic conditions, effectively balancing mission performance and safety. Future work will extend this approach to missions with

varied objectives and constraints, such as Ice-Sat2, to further confirm its versatility and practical applicability.

## REFERENCES

- [1] H. Save, J. Ries, S. Bettadpur, P. Nagel, and N. Pie, "Orbit management during solar cycle 25 for optimal science on GRACE-FO mission," *AAS/AIAA Spaceflight Mechanics Meeting*, 2023.
- [2] M. L. Puterman, *Markov decision processes: discrete stochastic dynamic programming*. John Wiley & Sons, 2014.
- [3] R. P. Kornfeld, B. W. Arnold, M. A. Gross, N. T. Dahya, W. M. Klipstein, P. F. Gath, and S. Bettadpur, "GRACE-FO: the gravity recovery and climate experiment follow-on mission," *Journal of spacecraft and rockets*, Vol. 56, No. 3, 2019, pp. 931–951.
- [4] D. Eddy and M. Kochenderfer, "Markov decision processes for multi-objective satellite task planning," *2020 IEEE Aerospace Conference*, IEEE, 2020, pp. 1–12.
- [5] M. Isaji and K. Ho, "Integrated Space Mission Planning Under Uncertainty via Stochastic and Decomposition-Based Optimization," *AIAA AVIATION FORUM AND ASCEND 2024*, 2024, p. 4816.
- [6] M. Vasile, "Robust mission design through evidence theory and multiagent collaborative search," *Annals of the New York Academy of Sciences*, Vol. 1065, No. 1, 2005, pp. 152–173.
- [7] M. Ahmadi, M. Ono, M. D. Ingham, R. M. Murray, and A. D. Ames, "Risk-averse planning under uncertainty," *2020 American Control Conference (ACC)*, IEEE, 2020, pp. 3305–3312.
- [8] C. Baier and J.-P. Katoen, *Principles of model checking*. MIT press, 2008.
- [9] K. Y. Rozier, "Linear temporal logic symbolic model checking," *Computer Science Review*, Vol. 5, No. 2, 2011, pp. 163–203.
- [10] V. Forejt, M. Kwiatkowska, G. Norman, and D. Parker, "Automated verification techniques for probabilistic systems," *Formal Methods for Eternal Networked Software Systems: 11th International School on Formal Methods for the Design of Computer, Communication and Software Systems, SFM 2011, Bertinoro, Italy, June 13-18, 2011. Advanced Lectures 11*, 2011, pp. 53–113.
- [11] J. Picone, A. Hedin, D. P. Drob, and A. Aikin, "NRLMSISE-00 empirical model of the atmosphere: Statistical comparisons and scientific issues," *Journal of Geophysical Research: Space Physics*, Vol. 107, No. A12, 2002, pp. SIA–15.
- [12] J. T. Emmert, D. P. Drob, J. M. Picone, D. E. Siskind, M. Jones Jr., M. G. Mlynczak, P. F. Bernath, X. Chu, E. Doornbos, B. Funke, L. P. Goncharenko, M. E. Hervig, M. J. Schwartz, P. E. Sheese, F. Vargas, B. P. Williams, and T. Yuan, "NRLMSIS 2.0: A Whole-Atmosphere Empirical Model of Temperature and Neutral Species Densities," *Earth and Space Science*, Vol. 8, 2021, 10.1029/2020EA001321.
- [13] J. T. Emmert, M. Jones Jr, D. E. Siskind, D. P. Drob, J. M. Picone, M. H. Stevens, S. M. Bailey, S. Bender, P. F. Bernath, B. Funke, M. E. Hervig, and K. Pérot, "NRLMSIS 2.1: An Empirical Model of Nitric Oxide Incorporated Into MSIS," *Journal of Geophysical Research: Space Physics*, Vol. 127, No. 10, 2022, 10.1029/2022JA030896.
- [14] M. Miesch, "Solar Cycle Progression Updated Prediction (Experimental): Validation Document," 2024.
- [15] J. E. Prussing and B. A. Conway, *Orbital mechanics*. Oxford University Press, USA, 1993.
- [16] B. D. Tapley, S. Bettadpur, M. Watkins, and C. Reigber, "The gravity recovery and climate experiment: Mission overview and early results," *Geophysical research letters*, Vol. 31, No. 9, 2004.
- [17] F. W. Landerer, F. M. Flechtner, H. Save, F. H. Webb, T. Bandikova, W. I. Bertiger, S. V. Bettadpur, S. H. Byun, C. Dahle, H. Dobslaw, *et al.*, "Extending the global mass change data record: GRACE Follow-On instrument and science data performance," *Geophysical Research Letters*, Vol. 47, No. 12, 2020, p. e2020GL088306.
- [18] N. Pie and B. E. Schutz, "Subcycle analysis for ICESat's repeat groundtrack orbits and application to phasing maneuvers," *The Journal of the Astronautical Sciences*, Vol. 56, No. 3, 2008, pp. 325–340.
- [19] J. Klokočník, J. Kostelecký, and R. Gooding, "On fine orbit selection for particular geodetic and oceanographic missions involving passage through resonances," *Journal of Geodesy*, Vol. 77, 2003, pp. 30–40.